processes

MDPI

Article

DEM Investigation on the Flow and Heat Transmission Characteristics of Multi-Size Particles Mixed Flow in Moving Bed

Wenbo Cao [1], Fengxia Zhang [2], Jianhang Hu [1,*], Shiliang Yang [1], Huili Liu [1] and Hua Wang [1]

[1] Engineering Research Center of the Ministry of Education for Metallurgical Energy Conservation and Emission Reduction, Kunming University of Science and Technology, Kunming 650093, China; caowenbo10@163.com (W.C.)
[2] Kunming Metallurgy College, Kunming 650033, China; fengxia_zhang@163.com
* Correspondence: jianhang@kust.edu.cn

Abstract: The moving bed heat exchanger (MBHE) has been widely applied in the recovery of waste heat of industrial particles. Currently, investigations focus on uniform-size particles in the MBHE, but few studies are conducted on multi-size particles produced by industrial granulation. Therefore, based on the discrete element method (DEM), the heat transmission model of multi-size particles is established, and flow and heat transmission processes of typically normal distribution particles in the MBHE are studied. In conclusion, there are significant differences in particles tangential velocity and contact number in local regions of a heat exchanger pipe, resulting in different local heat transmission coefficients. In addition, the increases in outlet particle velocity and inlet particle temperature significantly enhance the heat transmission. When the outlet particle velocity grows from 1 mm/s to 5 mm/s, the overall heat transmission coefficient increases by 36.4%, and as the inlet particle temperature rises from 473 K to 873 K, the overall heat transmission coefficient increases by 16.1%.

Keywords: moving bed heat exchanger; waste heat recovery; multi-size particle; discrete element method

check for updates

Citation: Cao, W.; Zhang, F.; Hu, J.; Yang, S.; Liu, H.; Wang, H. DEM Investigation on the Flow and Heat Transmission Characteristics of Multi-Size Particles Mixed Flow in Moving Bed. *Processes* **2024**, *12*, 408. https://doi.org/10.3390/pr12020408

Academic Editor: Udo Fritsching

Received: 21 January 2024
Revised: 9 February 2024
Accepted: 16 February 2024
Published: 18 February 2024

1. Introduction

Vital parts of the national economy, metallurgy, cement, and heat power industries play significant roles in promoting economic growth and upgrading people's living standards [1–3]. However, the development of these industries needs to consume large amounts of energy and will release large quantities of pollutants including carbon dioxide [4,5], which will not only aggravate the global energy crisis, but also contribute to global warming and seriously hinder the sustainable development of human beings [6]. Therefore, it is of profound significance to realize the human-shared vision of emission peak and carbon neutrality through promoting the energy saving, consumption diminution and green low-carbon development of these excessive-energy expenditure and high-polluted enterprises [7].

Studies have shown that these industries generate large quantities of high-temperature solid materials, such as copper slag, steel slag, blast furnace slag, sintered ore, fly ash, etc., which contain abundant waste heat resources [8,9]. Taking copper slag as an example, its heat content is about 1.13 GJ/t [10], while the world's refined copper production in 2022 was about 25.08 Mt, and each ton of refined copper produces about 2.2 t of copper slag; so, the heat content is equivalent to about 2.1 million tce, which has a considerable waste heat recovery value [11]. Therefore, considerable studies in recovering waste heat from particles have been carried out by scholars at home and abroad; furthermore, a variety of approaches including fluidized bed, packed bed, and moving bed have been put forward [8].

The fluidized bed has the advantages of highly efficient heat transmission rate, uniform particle temperature and concentration distribution, and a wide adjustment range of operating parameters, which has been widely used in the fields of energy, metallurgy, and chemical industries [12,13]. Nonetheless, the fluidized bed has not been widely applied in recovering waste heat due to its high energy consumption and limited particle diameter [8]. As for the packed bed, it is suitable for large size particles and has been applied to annular coolers and grate coolers. However, because of the high gas velocity and limited bed height, the gas and solid phase cannot reach heat equilibrium at the outlet, and it is easy to produce secondary dust pollution, that is why the application range in industry is limited [8,14].

The particles in the moving bed heat exchanger (MBHE) rely on their own gravity to accumulate and fall down and then collide with the heat exchanger pipe or plate and shell to transfer heat with the fluid medium in them. Therefore, it has the merits of a low-energy consumption, no secondary pollution, and a high waste heat recovery efficiency [15]. Compared with the plate and shell heat exchanger, the tubular heat exchanger can withstand higher pressure fluids [16], which make it possible to produce steam with high temperature and high pressure, and then generate electricity through steam turbines [17]; therefore, it has broad application prospects. At present, this technology has been applied in the sintering pellet waste heat recovery process of a steel plant in Northeast China, and the net power generation per ton of sintering pellet reaches 16 kW·h. However, there are still some technical problems in the large-scale engineering application of this technology. Therefore, scholars in this field have conducted many studies.

Aiming at the problem of heat transmission deterioration caused by the void region and stagnation region around the heat exchanger pipe, Tian et al. [18] changed the circular pipe to an elliptical pipe or hexagonal pipe, and then increased the average heat transmission coefficient by 17.2% and 20.5%, respectively. Guo et al. [19] investigated the influence of the inclination angle of the heat exchanger pipe on heat transmission and noticed that the heat transmission area increased as the inclination angle increased, resulting in a significant heat transmission increase, but the heat transmission coefficient in local regions was uncertain. It was recommended that the inclination angle was between 15° and 37.5°. Shen et al. [20] studied the influence of particle diameter, the coefficient of static friction and density on heat transmission. It was found that the particle diameter had the greatest influence on heat transmission. When the diameter increased to 4 mm from 2 mm, the mean coefficient of effective heat transmission of the heat exchanger pipe decreased by 17.2%. The rise of the particle static friction coefficient would lead to the increase in the void area and the reduction in the contact number, while the particle density had little effect. Qiu et al. [21] investigated the influence of the arrangement and quantity of heat exchanger pipes on heat transmission. It was found that the heat transmission effectiveness of the aligned arrangement was poorer than that of the staggered arrangement, and increasing the quantity of heat exchanger pipes could effectively improve the efficiency of waste heat recovery.

Above all, most of the current studies are concentrated on the waste heat recovery of particles with the uniform size in MBHE; nevertheless, in the practical industrial production, the particles produced by mechanical crushing, air quenching, and centrifugal granulation [22] often have complex size distribution [10,23]. Although Zhang [24] and Qiu [25] investigated the heat transmission of particles with continuous uniform distribution and normal distribution in the moving bed, respectively, their object was an air–solid moving bed heat exchanger, which depended on direct convective heat transmission between air and particles. Zhang [26] studied multi-size particles in the moving bed tubular heat exchanger, but only limited to binary particle sizes.

Therefore, in this study, the discrete element method (DEM) was used to simulate the characteristics of flow and heat transmission of high-temperature particles with a normal distribution characteristic generated in the industrial production process in a single-pipe MBHE. The effects of two key process parameters such as outlet particle velocity and inlet particle temperature on the contact number, the average tangential velocity of particles surrounding the heat exchanger pipe, the local and overall heat transmission coefficients of the heat exchanger pipe, and the temperature distribution of particles surrounding the heat exchanger pipe were analyzed. The findings provided technical guidance for waste heat recovery from industrial particles with complex size distribution.

2. Physical and Mathematical Model Description

2.1. Physical Model

Simulation of the particle flow in an industrial-scale MBHE using the DEM requires large quantities of computational resources; therefore, the model is reduced to the scale of a single-pipe MBHE in order to shorten the computational time with the limited arithmetic resources. The physical model consists of a rectangular particle flow channel (L × W × H) and a cylindrical heat exchanger pipe (L × D), as shown in Figure 1. The boundary condition of the model's top is set as the mass inflow, the bottom is set as the velocity boundary condition, and the boundary conditions of the remaining four walls and the heat exchanger pipe wall are set as the no-slip. The four walls are adiabatic, and the pipe wall temperature is a constant value of T_{pipe} = 298 K. The particle flow enters the flow channel from the top of the model with a set mass flow rate, then falls under gravity and exchanges heat with the cold pipe wall, and finally exits from the bottom of the model with a set velocity. During this process, dynamic conservation of the total particles mass in the heat exchanger is maintained by setting the mass flow rate of the inlet particles and the velocity of the outlet particles. The particle size in this study has a normal distribution with the probability density function shown in Equation (1) [27], which is based on a the number rather than mass or volume and it represents the relative frequency of particles of different sizes in terms of the number. It describes how many particles are present at each size interval. The mean particle size is μ = 2 mm, calculated as in Equation (2) [28], with a standard deviation of σ = 0.5 mm, calculated as in Equation (3) [29], and the particle diameter is limited to 1~3 mm [8]. The simulation parameters are listed in Table 1.

Table 1. Physical parameters for DEM simulation.

Category	Physical Parameters	Value
MBHE geometry		
	L × W × H, mm	63 × 27 × 90
Heat exchanger pipe		
	L × D, mm	27 × 40
	k_{pipe}, W·m^{-1}·K^{-1}	18
	T_{pipe}, K	298
Particle		
	d, mm	1~3
	k_s, W·m^{-1}·K^{-1}	1.0
	c_p, J·kg^{-1}·K^{-1}	780
	v_{out}, mm/s	1, 2, 3, 4, 5
	T_{inlet}, K	473, 573, 673, 773, 873
	Density, kg/m^3	2700
Gas		
	k_g, W·m^{-1}·K^{-1}	$k_g = 0.0252\sqrt{T_g/300}$
Contact parameters		
	Young's modulus (particle), Pa	1×10^8
	Young's modulus (heat exchanger pipe), Pa	1×10^{11}
	Poisson ratio (particle)	0.3
	Poisson ratio (heat exchanger pipe)	0.3
	Coulomb friction coefficient (particle-particle)	0.3
	Coulomb friction coefficient (particle-heat exchanger pipe)	0.25
	Rolling friction coefficient (particle-particle)	0.18

Table 1. *Cont.*

Category	Physical Parameters	Value
	Rolling friction coefficient (particle-heat exchanger pipe)	0.1
	Normal spring constant (particle-particle), N/m	800
	Normal spring constant (particle-heat exchanger pipe), N/m	800
	Spring tan/norm ratio (particle-particle)	2/7
	Spring tan/norm ratio (particle-heat exchanger pipe)	2/7
	Damping tan/norm ratio (particle-particle)	0.5
	Damping tan/norm ratio (particle-heat exchanger pipe)	0.5
	Restitution coefficient (particle)	0.5
	Restitution coefficient (heat exchanger pipe)	0.3
	Grid size, mm	3 × 3 × 3

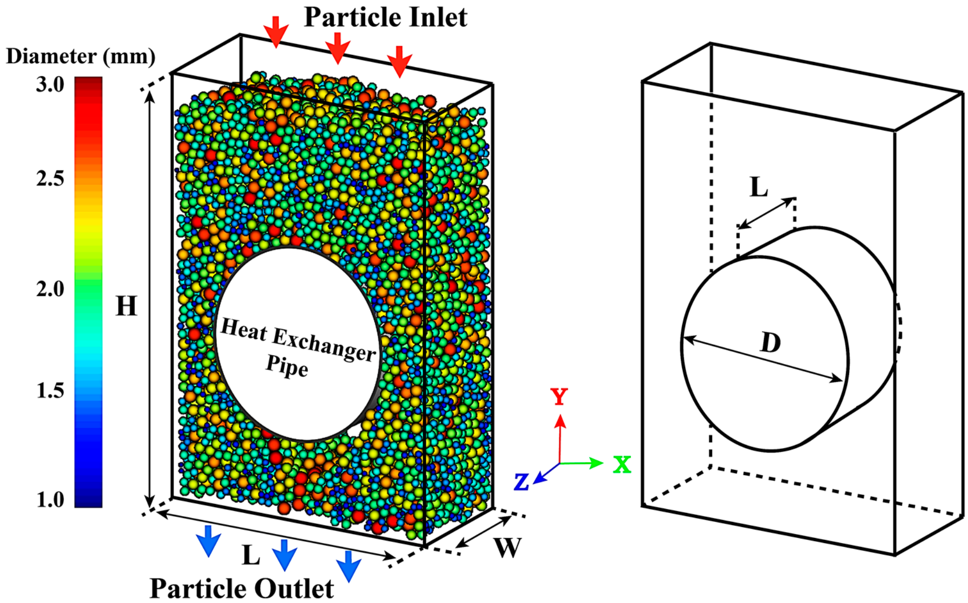

Figure 1. Physical model of the single-pipe MBHE.

$$f(d) = \frac{1}{\sigma\sqrt{2\pi}} \exp\left[-\frac{(d-\mu)^2}{2\sigma^2}\right] \quad (1)$$

$$\mu = \frac{1}{n}\sum_{i=1}^{n}(n_i d_i) \quad (2)$$

$$\sigma = \sqrt{\frac{1}{n}\sum_{i=1}^{n}(d_i-\mu)^2} \quad (3)$$

2.2. Mathematical Model

2.2.1. Dynamics Model

Cundall and Strack initially proposed the DEM [30] and applied it to the study of rock mechanics, and then gradually extended to the field of powder engineering. Common DEM models are hard-sphere and soft-sphere. In the hard-sphere model, the hardness of the particle is considered to be infinite, and the collision between the particles is assumed to be instantaneous and the particles do not deform during the collision [31]. Whereas in the soft-sphere model, the particles could deform slightly during the interaction and the forces between them are determined based on the degree of deformation. Compared with the hard-sphere model, the soft-sphere model is more suitable for the dense-phase granule system with frequent contact [32], so the soft-sphere model is applied in this investigation. In addition, the linear spring dashpot (LSD) collision model is chosen for quicker solving.

The particle undergoes translational and rotational movements under the action of forces and moments, which include gravity, elasticity, friction, damping force, and air drag force [33]. However, in this study, the particles are closely packed in the flow channel under gravity and the relative velocity between particles and air is quite slow, which makes the influence of air drag force very weak. Therefore, the air drag force is negligible compared to the strong interaction force between particles [34]. The motion equations of the particle can be written as [35]:

$$m_i \frac{dv_i}{dt} = \sum_{j=1}^{n_c} (F_{n,ij} + F_{t,ij}) + m_i g \tag{4}$$

$$I_i \frac{d\omega_i}{dt} = \sum_{j=1}^{n_c} (T_{t,ij} + T_{r,ij}) \tag{5}$$

where m_i, I_i, v_i and ω_i denote the mass, inertial moment, translatory velocity and angular velocity of particle i, respectively. Where t is the time, n_c is the quantity of particles which contact particle i, j is the particle index, and g is the gravitational acceleration. In addition, $F_{n,ij}$, $F_{t,ij}$, $T_{t,ij}$, and $T_{r,ij}$ represent the normal force, the tangential force, the tangential torque and the rolling friction torque, respectively. The collision model of particle–particle is shown in Figure 2a.

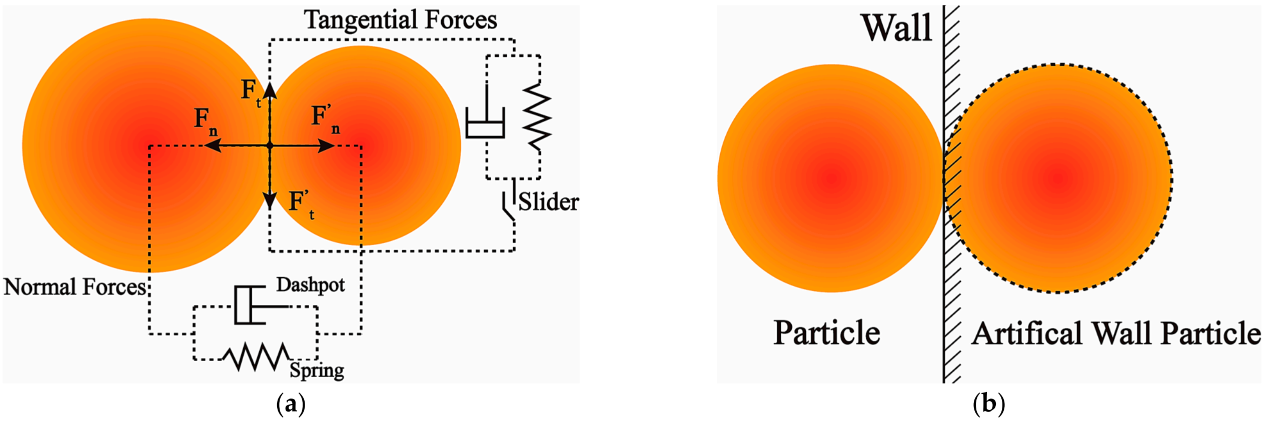

Figure 2. Schematic diagrams of collision models: (**a**) particle–particle; (**b**) particle–heat exchanger pipe wall.

When a particle collides with a wall, a virtual particle named the artificial wall particle is used to act as the wall, so that the interaction force can be calculated in the same way as particle–particle collision. The size of the artificial wall particle is exactly the same as the particle that collides with the wall, but its physical properties are specified by the wall. When the particle ends its collision with the wall, the artificial wall particle will be immediately removed. In addition, this process is presented in Figure 2b [36].

2.2.2. Thermodynamics Model

In general, the heat transmission mechanisms of particles within MBHE consist of three types: conduction, convection, and radiation [37]. However, in this study, convection heat transmission could be ignored since the particles flow is very dense and the relative velocity is low, which results in very weak convection heat transmission between particles and the air and between the air and the pipe [38]. In addition, the heat transmission by radiation is two orders lower than that by conduction when particle temperature is below 800 °C, according to the study of heat exchanger pipes for waste heat recovery from calcined oil coke by Zheng et al. [39]. Also, since this study focuses on the role of the main heat transmission mechanism within MBHE and the particle temperature is not higher than 600 °C, the influence of heat radiation is ignored. Additionally, the frictions and collisions of particle–particle and particle–pipe cause changes in internal energy, but they are not considered due to the low speed of the particles, which produces little effect.

Heat conduction in this investigation consists of two approaches, one is through contact heat conduction including particle–particle (p-p) and particle–heat exchanger pipe wall (p-w), and the other is through air-film heat conduction, including particle–fluid–particle (p-f-p) and particle–fluid–heat exchanger pipe wall (p-f-w). For the purpose of studying the heat conduction between particles with different sizes and physical properties, Musser [36] improved the contact heat conduction model proposed by Batchelor and O'Brien [40] as well as the model of air-film heat conduction put forward by Rong and Horio [41]. The improved model contains the following assumptions: (1) Every particle is enwrapped by an air film with a thickness of $\delta_g = 0.1d$ [42]; (2) The air-film heat conduction occurs when the air film of one particle is in contact with the superficies of the other particles, and when the particles are in contact, the air-film heat conduction and the contact heat conduction occur simultaneously; (3) The heat transmission path is parallel to the connection line in the center of the particles. In addition, the heat conduction model schematic between particles is shown in Figure 3a. On this basis, Morris [43] developed a heat conduction model for a heat exchanger pipe wall with particle, while the schematic of this model is presented in Figure 3b.

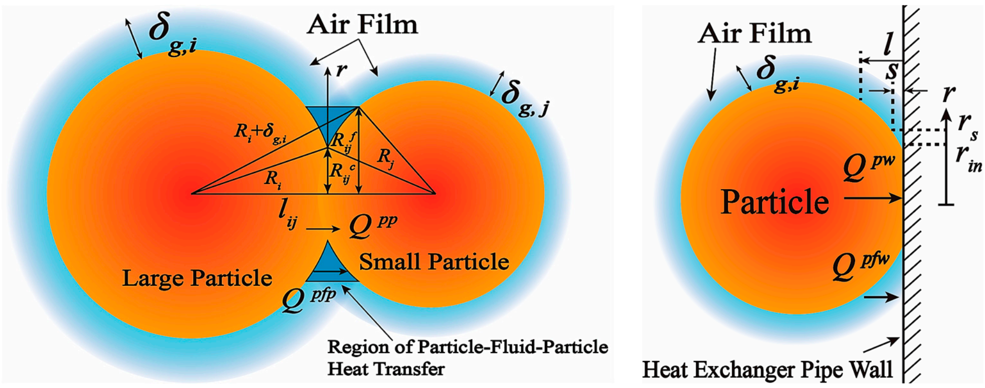

(**a**) (**b**)

Figure 3. Schematic of heat transmission models: (**a**) particle–particle; (**b**) particle–heat exchanger pipe wall.

The equation for energy conservation of particle is written as [44]:

$$m_i c_{p,i} \frac{dT_i}{dt} = \sum_{j=1}^{n_c} \left(Q_{ij}{}^{pp} + Q_{ij}{}^{pfp} \right) + Q^{pw} + Q^{pfw} \tag{6}$$

where $c_{p,i}$ represents the specific heat capacity of particle i, T_i denotes the temperature of particle i, $Q_{ij}{}^{pp}$ and $Q_{ij}{}^{pfp}$ represent the heat transmission rates between particle i and particle j through contact heat conduction and air-film heat conduction, respectively. While Q^{pw} and Q^{pfw} denote the heat transmission rates between the particle and heat exchanger pipe wall through contact heat conduction and air-film heat conduction, respectively. The equation for particle contact heat conduction is defined as [40]:

$$Q_{ij}{}^{pp} = \frac{4k_i k_j}{k_i + k_j} R_{ij}{}^{c} (T_j - T_i) \tag{7}$$

where k_i and k_j represent the heat conductivity of particle i and particle j, respectively, ${R_{ij}}^c$ represents the circular contact zone radius between particles, while T_j represents the temperature of particle j. The formula for air-film heat conduction of particles is determined as [41]:

$$Q_{ij}{}^{pfp} = k_g(T_j - T_i)\int_{R_{ij}{}^c}^{R_{ij}{}^f} \frac{2\pi r}{l_{ij} - \left(\left({R_i}^2 - r^2\right)^{1/2} + \left({R_j}^2 - r^2\right)^{1/2}\right)}dr \tag{8}$$

where k_g represents the air heat conductivity, ${R_{ij}}^f$ represents the upper limit distance of the air-film heat conduction, ${R_{ij}}^c$ and ${R_{ij}}^f$ can be calculated according to Equations (9) and (10), respectively. R_i and R_j represent the radius of the particle i and particle j, respectively. R_{max} and R_{min} denote the maximum and minimum radius of particle i and particle j described as Equations (11) and (12), respectively. l_{ij} denotes the central distance between particle i and particle j, r represents the radial distance, and δ_{max} denotes the maximum air-film thickness of particle i and particle j. The equations are as follows:

$$R_{ij}{}^c = \begin{cases} 0 & l_{ij} > (R_i + R_j) \\ \sqrt{{R_{max}}^2 - \left(\frac{{R_{max}}^2 - {R_{min}}^2 + {l_{ij}}^2}{2l_{ij}}\right)^2} & l_{ij} \le (R_i + R_j) \end{cases} \tag{9}$$

$$R_{ij}{}^f = \sqrt{(R_{max} + \delta_{max})^2 - \left(\frac{(R_{max} + \delta_{max})^2 - {R_{min}}^2 + {l_{ij}}^2}{2l_{ij}}\right)^2} \tag{10}$$

$$R_{max} = \max\{R_i, R_j\} \tag{11}$$

$$R_{min} = \min\{R_i, R_j\} \tag{12}$$

The equation for contact heat conduction between the heat exchanger pipe and particle is expressed as:

$$Q^{pw} = \frac{4k_i k_{pipe}}{k_i + k_{pipe}} R^c (T_{pipe} - T_i) \tag{13}$$

where k_{pipe} represents the heat conductivity of the heat exchanger pipe, T_{pipe} represents the temperature of the heat exchanger pipe, and R^c is the contact area radius between particle and heat exchanger pipe wall. The equation for air-film heat conduction between particle and heat exchanger pipe is defined as follows [44]:

$$Q^{pfw} = (T_{pipe} - T_i)\int_{r_{in}}^{r_{out}} \frac{2k_g \pi r}{\max(s, l)}dr \tag{14}$$

where r_{in} is the radial distance associated with the contact area between particle and heat exchanger pipe, r_{out} denotes the distance where particle air film intersects the heat exchanger pipe wall, s denotes the minimum conduction distance, and l is the normal distance from the pipe wall to particle surface, which can be calculated according to Equation (15) as follows:

$$l = R_i - \delta_c - \sqrt{R_i^2 - r^2} \tag{15}$$

where δ_c is the overlap between the particle and heat exchanger pipe wall.

2.3. Model Validation

For the purpose of verifying the precision of the model prediction results, Zhang [45] and Okazaki's [46] experiments were simulated separately in this study. Zhang investigated the effects of the size as well as the residence time of high temperature quartz sand on a heat transmission coefficient in the MBHE, and the experimental result can be used to prove the precision of the granular heat transmission model for the same particle size. While the precision of this model under different particle size conditions can be verified by Okazaki's experimental result. Figure 4a,b show the simulation and experimental results, and it can be seen that for the same particle size from Figure 4a, the maximum deviation between the simulation prediction and the experimental result is 9.5% and the average deviation is 4.3%. From Figure 4b, it can be seen that for particles of different sizes the maximal deviation between model predictions and experimental results is 12.8% with an average deviation of 7.6%. As a conclusion, in both cases, the predictions of the heat transmission model agree with the results of experiments well, so this model could be effectively applied to predict the heat transmission of multi-size particles in the MBHE.

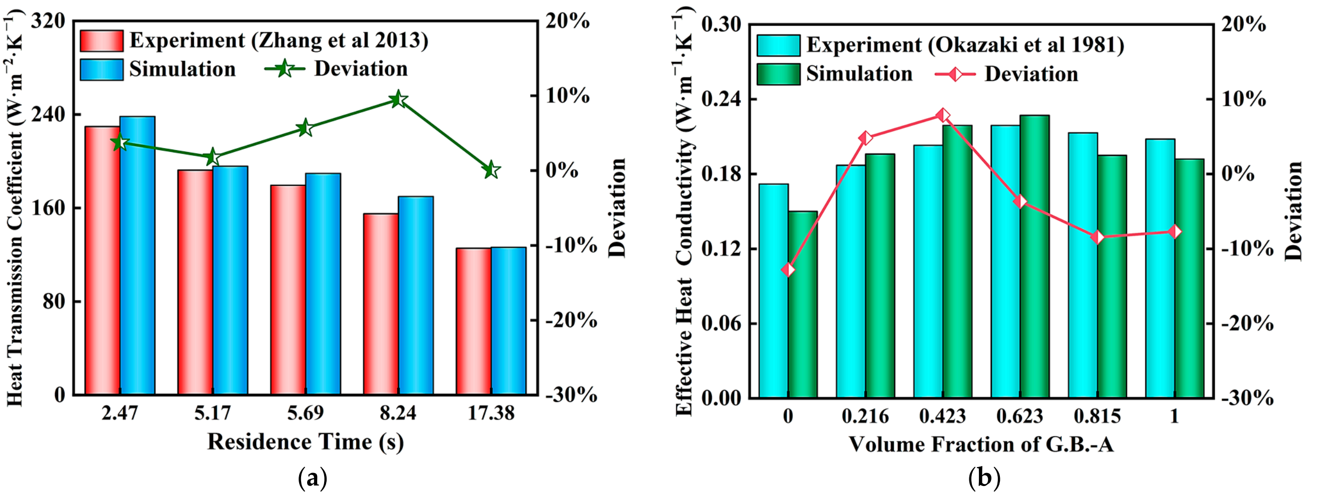

Figure 4. Result comparison between simulations and experiments: (**a**) heat transmission coefficient of uniform-size particles [45]; (**b**) effective heat conductivity of multi-size particles [46].

3. Results and Discussion

The flow characteristics of particles in the MBHE are quite complex. The outcomes of the experiments and simulations of Dai [47] and Bartsch et al. [16] showed that there were significant differences in particle flow in different regions around heat exchanger pipe. For example, at the upper part of the heat exchanger pipe, the flow velocity of particles was slow and there was a typical stagnation zone, while at the side region, the particles flow velocity was fast, and there was an apparent void area at its bottom. Therefore, the heat transmission characteristics in various regions of the heat exchanger pipe would be more complicated. Thus, Zhang et al. [26] radially divided the pipe into three regions, top, side, and bottom, to analyze.

While in this study, the heat exchanger pipe was divided into six regions in the radial direction according to the angle, as shown in Figure 5, and the angle of each region was 30°. However, the void region resulted in almost no particles in the 150~180° region, thus only the 0~150° region was focused on. When the particle flow reached a relatively steady state, the time–mean values of all particles in the region were extracted for analysis. For the particle flow characteristics, the particle tangential velocity along the pipe wall in the XY plane as well as the contact number between the pipe and particles were investigated. As for the heat transmission characteristics, the overall and local heat transmission coefficients for contact and air-film heat conduction between particles and the heat exchanger pipe were investigated, respectively. In addition, the temperature distribution of the particles surrounding the heat exchanger pipe was also studied. The heat transmission coefficient between particles and heat exchanger pipe could be calculated as follows [48]:

$$h = \frac{Q}{A_{pipe}(T_{inlet} - T_{pipe})} \quad (16)$$

where h represents heat transmission coefficient, Q denotes the heat transmission rate, A_{pipe} is the surface area of heat exchanger pipe, and T_{inlet} and T_{pipe} are inlet particle temperature and temperature of heat exchanger pipe, respectively.

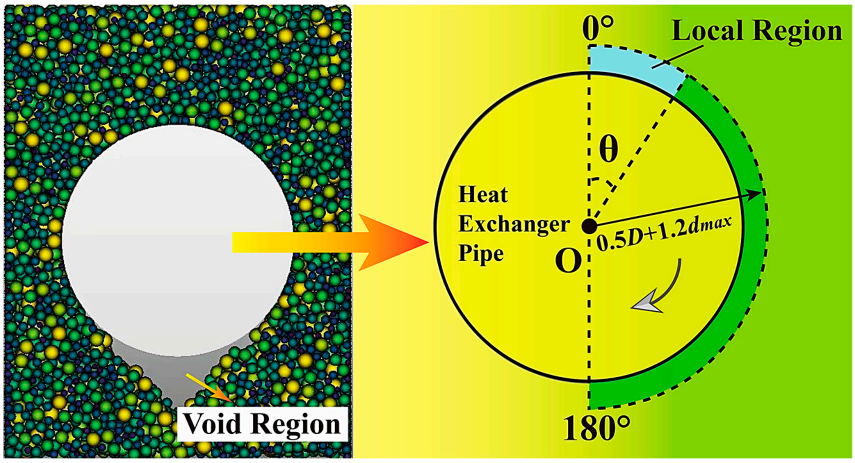

Figure 5. Local region division of heat exchanger pipe.

3.1. Analysis of Particles Flow Characteristics

The velocity field of the particles in MBHE is significantly affected by the heat exchanger pipe, and the flow characteristics of particles around the pipe are directly associated with the heat transmission effectiveness, so it is crucial to analyze the particle flow characteristics in detail. v_{tan} refers to the magnitude of the particle's average tangential velocity in the region presented in Figure 5 in the XY plane along the heat exchanger pipe, which reflects the speed of particle renewal on the heat exchanger pipe surface. Initially, the variation in the particle's average tangential velocity v_{tan} with the outlet particle flow velocity v_{out} is investigated for five local regions of the heat exchanger pipe as well as for the overall pipe. From Figure 6, it can be seen that at the same v_{out}, the v_{tan} of local regions gradually increases with the rise of angle. The v_{tan} in the region of 0~30° is the smallest, while the v_{tan} in the region of 120~150° is the largest. This is attributed to the fact that when the particles flow downward under the action of gravity, the component forces of the support force and friction force on the particles from the upper part of the pipe wall in the Y-axis direction are just opposite to the gravity, and therefore obstructs the particles from flowing downward. Whereas, as the angle of the region increases, the component forces decrease, so the obstruction of the pipe wall to the particles is becoming smaller and smaller, resulting in the larger v_{tan}. With the increase of v_{out}, the local and overall v_{tan} of heat exchanger pipe also increases steadily. When v_{out} rises from 1 mm/s to 5 mm/s [8], the overall v_{tan} of heat exchanger pipe rises from 2.7 mm/s to 19.9 mm/s.

N_c represents the number of particles which contact the pipe per unit area in each time step [49]. In general, the larger N_c implies a higher quantity of particles exchanging heat with the heat exchanger pipe and a better contact situation. The variation in the particle's contact number N_c of the five local regions and the overall of the heat exchanger pipe with the outlet particle velocity v_{out} is shown in Figure 7. It could be observed that under the same v_{out}, the change tendency of N_c in local regions is opposite to that of v_{tan}. As the angle increases, the N_c of local regions decreases gradually, but decreases sharply in the region of 120~150°. Among these five regions, N_c is the largest in the region of 0~30° and the smallest in the region of 120~150°, which is also due to the hindering effect on the particles from the upper part of the pipe wall, leading to the formation of a dense accumulation of particles at the top of the pipe wall and thus N_c reaches its maximum value. Whereas when the particles arrive at the lower part of the pipe wall, the hindering effect on the particles becomes smaller, which makes the particle flow looser, leading to the smaller N_c. In addition, with the increase of v_{out}, the N_c of the five local regions and the overall of heat exchanger pipe fluctuates slightly and remains basically steady. This is because the particles flow is not continuous, so there is a certain fluctuation in the data [34]. At the same time, it also indicates that v_{out} has almost no effect on N_c in the range of 1~5 mm/s.

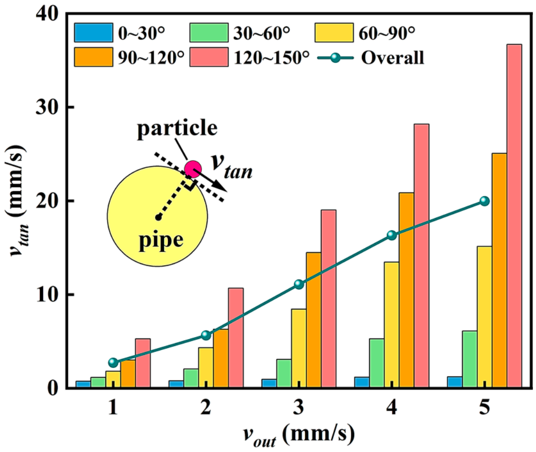

Figure 6. Variation in the overall and local particles average tangential velocity along heat exchanger pipe in the XY plane with the outlet particle velocity.

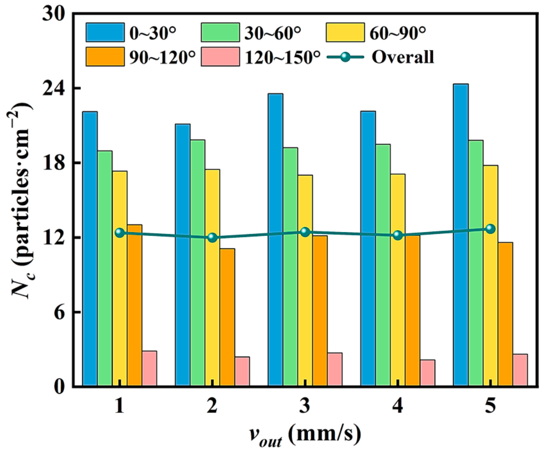

Figure 7. Variation in the local and overall particles contact number of heat exchanger pipe with the outlet particle velocity.

3.2. Analysis of Particles Heat Transmission Characteristics

3.2.1. The Influence of Outlet Particle Velocity

The heat transmission characteristics of particles in the MBHE are significantly affected by the particle flow characteristics. The research in Section 3.1 indicates that the outlet particle velocity directly affects the particles average tangential velocity along the surface of the heat exchanger pipe in the XY plane. Therefore, the effect of the outlet velocity of particles on heat transmission between particles and the heat exchanger pipe is minutely studied (T_{inlet} = 873 K).

Firstly, the change in the overall heat transmission coefficient $h_{overall}$ of the heat exchanger pipe with the outlet particle velocity v_{out} is investigated, including the heat transmission coefficient for the air-film heat conduction and the contact heat conduction. As presented in Figure 8, the $h_{overall}$ of both heat transmission approaches gradually increases with the rise of v_{out}. When v_{out} grows from 1 mm/s to 5 mm/s, the $h_{overall}$ for the air-film heat conduction increases by 37.4%, while the $h_{overall}$ for the contact heat conduction increases by 24.2%. The sum of the $h_{overall}$ of these two heat transmission approaches increases by 36.4%. It can be concluded that the rise of v_{out} has a considerable promoting impact on the $h_{overall}$ of the two heat transmission approaches.

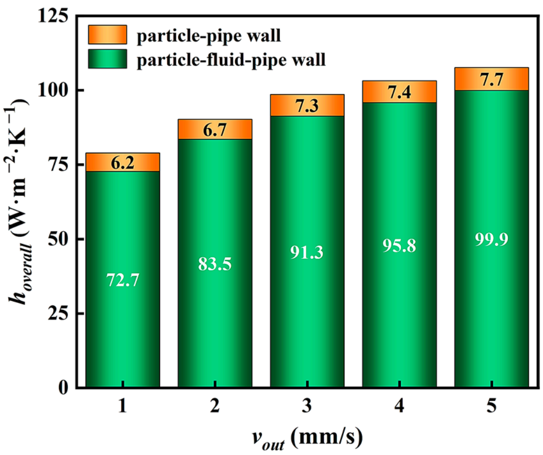

Figure 8. Variation in the overall heat transmission coefficient of heat exchanger pipe for the contact heat conduction and the air-film heat conduction with the outlet particle velocity.

The reason is that as the v_{out} increase, the update frequency of particles on the surface of the heat exchanger pipe is accelerated, which induces higher particle temperatures in the heat transmission process, thus it leads to the larger temperature contrast between particles and heat exchanger pipe, contributing to more heat transmission [50]. At the same time, the more rapid flow velocity implies that the particles have greater momentum, as a consequence, when they collide with the pipe wall, the deformation is larger, resulting in an increase in the contact area, which is conducive to heat transmission. In addition, it is also discovered that the air-film heat conduction contributes the most to $h_{overall}$ and plays a dominant role compared with the contact heat conduction. This is due to the fact that the hardness of the particles in this study is high, and the deformation during the collision is slight, resulting in a small heat transmission area, while the air-film heat conduction is almost unaffected by this. In contrast, the heat transmission area of air-film heat conduction is much larger than that of contact heat conduction, thus contributing to more heat transmission.

According to the results of Section 3.1, there are notable differences in the flow characteristics of particles in different local regions of the pipe wall. Whether the local v_{tan} or N_c could influence the heat transmission coefficient. Therefore, the effects of the outlet particles velocity v_{out} on the local heat transmission coefficient h_{local} ($h_{local} = h_{local\text{-}pw} + h_{local\text{-}pfw}$), the local heat transmission coefficient for the air-film heat conduction $h_{local\text{-}pfw}$, and the local heat transmission coefficient for contact heat conduction $h_{local\text{-}pw}$ are also analyzed, respectively.

Figure 9a shows the variation in the local heat transmission coefficient h_{local} of the heat exchanger pipe with the outlet particle velocity v_{out}. It can be observed that with the rise of v_{out}, except for the 120~150° region, the h_{local} in other regions increases significantly, while increasing slightly in the 120~150° region. As the v_{out} rises from 1 mm/s to 5 mm/s, the h_{local} of the five local regions increases by 38.3%, 46.6%, 39.2%, 36.6%, and 16.1% from 0° to 150°, respectively. Among them, the rise of h_{local} in the 30~60° region is the largest, the rises of h_{local} in the three regions of 0~30°, 60~90°, and 90~120° are slightly smaller and closer, and the rise of h_{local} in the 120~150° region is the smallest.

This is since the increase of v_{out} remarkably improves the v_{tan} in each region and accelerates the update frequency of the particles, which causes the particle flow to impact the upstream pipe wall with greater momentum, leading to a greater collision deformation, enlarging the heat transmission area, and effectively improving the heat transmission coefficient. However, for the downstream of the pipe wall, the particles flow moves away from the pipe wall as a whole, so the increase of v_{out} only improves the particles update frequency but does not effectively increase the impact deformation of the particles and pipe wall, as a consequence, the rise of heat transmission coefficient in these areas is small.

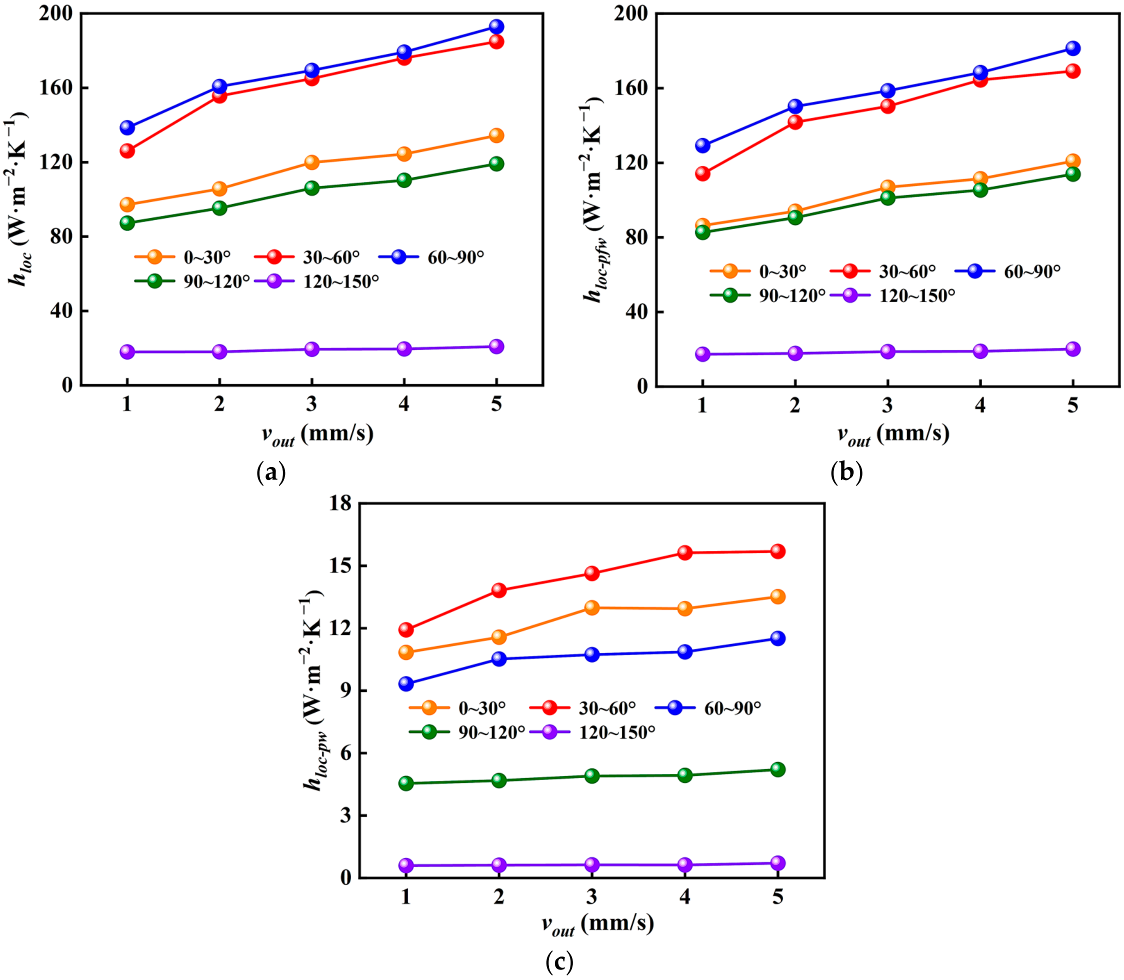

Figure 9. Variation in the local heat transmission coefficient of heat exchanger pipe with the outlet particle velocity: (**a**) for both of the air-film heat conduction and the contact heat conduction; (**b**) for the air-film heat conduction; (**c**) for the contact heat conduction.

From the perspective of the value of h_{local}, the h_{local} in the 30~60° and 60~90° regions are similar, so as in the 0~30° and 90~120° regions, while the h_{local} in the 120~150° region is relatively lower than that in the other four regions. Among the five regions, the 60~90° region has the largest h_{local}, while the 120~150° region has the smallest h_{local}, which are the outcomes of the comprehensive effects of v_{tan}, N_c, and other factors. For instance, the v_{tan} in the 0~30° region is the smallest, and the particles update frequency is the slowest, but the h_{local} in this region is at the medium level. This is because the N_c in this region is the largest, leading to the dense particle accumulation. This region is located in the upstream of the pipe wall; therefore, particles have a greater impact on it and generate a larger heat transmission area. Accordingly, under the comprehensive effects of these factors, the h_{local} in the 0~30° region is maintained at the medium level. On the contrary, the v_{tan} in the 120~150° region is the largest and the particle update frequency is the fastest, whereas the h_{local} in this region is the smallest, the reason is that the N_c in this region is very low, and the particles accumulation is quite loose. Furthermore, the region is located in the downstream of the pipe wall, so the impact of particles on the pipe wall is weak and the heat transmission area is quite small.

Figure 9b presents the change in the local heat transmission coefficient of the heat exchanger pipe for air-film heat conduction $h_{loc\text{-}pfw}$ with the outlet particle velocity v_{out}, and Figure 9c shows the variation in the local heat transmission coefficient of the heat exchanger pipe for contact heat conduction $h_{loc\text{-}pw}$ with outlet particle velocity v_{out}. It can be seen that the change trends of $h_{loc\text{-}pfw}$, $h_{loc\text{-}pw}$, and h_{local} in each region are almost the same; however, the relative size of $h_{loc\text{-}pfw}$ in each region is significantly different from that of $h_{loc\text{-}pw}$ in each region. In Figure 9b, the $h_{loc\text{-}pfw}$ of 0~30°, 30~60°, and 60~90° regions are ranked third, second, and first, respectively. Compared with Figure 9b, the $h_{loc\text{-}pw}$ of 60~90° region in Figure 9c decreases from the first to the third place, while the $h_{loc\text{-}pw}$ of 30~60° and 0~30° regions exceed that of the 60~90° region and rank first and second, respectively.

The reason is that as the angle increases, the interaction forces between the pipe wall and particles become weaker and weaker, causing the particles flow to become looser and looser. It is clear that this phenomenon will affect the contact heat conduction greater than the air-film heat conduction, because the air film expands the range of heat transmission, whereas the heat transmission range of the contact heat conduction is much smaller than that of the air-film heat conduction by contrast, resulting in the above differences. In Figure 9b, the $h_{loc\text{-}pfw}$ of 0~30° and 90~120° are highly close, while in Figure 9c, the divergence between $h_{loc\text{-}pw}$ of 90~120° and 0~30° increases sharply, which further proves that the influence of particle void fraction on contact heat conduction is much greater than that of air-film heat conduction.

The temperature distribution of particles surrounding the heat exchanger pipe reflects the particle heat transmission effect more intuitively. Figure 10 shows the change in the average particle temperature $T_{p,ave}$ of the five local regions and the overall region of the heat exchanger pipe with the outlet particle velocity v_{out}. It can be observed that with the increase of v_{out}, the $T_{p,ave}$ of both the five local regions and the overall region of the heat exchanger pipe increases, but the growth trend gradually slows down. When v_{out} rises to 5 mm/s from 1 mm/s, the $T_{p,ave}$ of the overall heat exchanger pipe rises from 609.7 K to 734.1 K, with a growth rate of 20.4%. This is due to the fact that as the v_{out} rises, particles flow faster through the surface of the heat exchanger pipe, resulting in shorter contact time, insufficient cooling, and less decrease in the particles temperature.

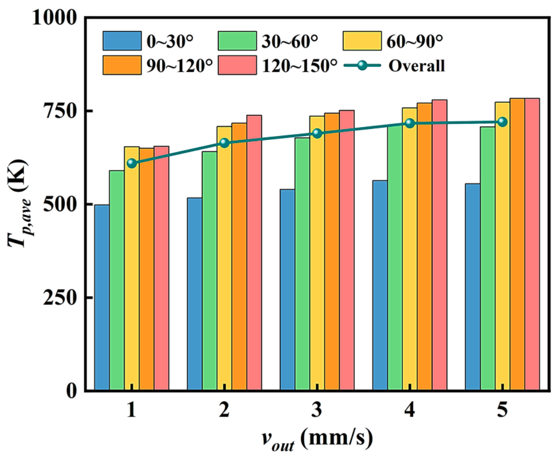

Figure 10. Variation in the local and overall particles average temperature of heat exchanger pipe with the outlet particle velocity.

When v_{out} stays constant, the $T_{p,ave}$ in the five local regions are compared, and it is found that the $T_{p,ave}$ in the 0~30° region is the lowest, and the $T_{p,ave}$ in the 30~60° region is a little higher than that in the 0~30° region, while the $T_{p,ave}$ in the other three regions are much larger and there is little difference between them. It can be interpreted that the v_{tan} in the 0~30° region is the smallest, the residence time is long, and the cooling is sufficient, therefore the temperature drops the most. As the angle increases, the v_{tan} rises, so the residence time shortens, and the particle temperature drops less. The reason why the $T_{p,ave}$ in the other three regions are similar is that although the particles which have been cooled in the upstream region will flow into these regions, the quantity of them is limited, and there are plenty of almost uncooled particles directly above, flowing into these regions. As a consequence, the particles that are from the upstream and have been cooled are heated in these regions by uncooled particles mentioned above, resulting in the particles temperature increase in these regions. A variety of the factors above induce the complex distribution of particle temperature, which can be observed more intuitively through Figure 11.

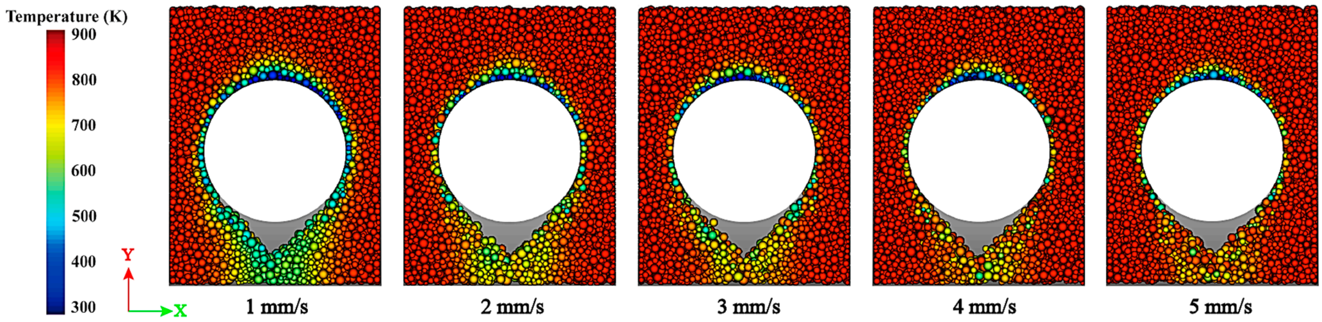

Figure 11. Particle temperature distribution in the XY plane of the single-pipe MBHE at different outlet particle velocity.

3.2.2. The Influence of the Inlet Particle Temperature

Zhang's [45] experimental and theoretical study showed that the heat transmission coefficient is closely related to the inlet particle temperature. In addition, the investigation of Qiu et al. [21] suggested that the inlet particle temperature also has significant influence on the heat recovery efficiency. Thus, the heat transmission characteristics between particle and the heat exchanger pipe at various inlet particle temperature are studied (v_{out} = 2 mm/s) in this section.

Similar to Section 3.2.1, firstly, the variation in the overall heat transmission coefficient of heat exchanger pipe $h_{overall}$ with the inlet particle temperature T_{inlet} is studied, including the above two heat transmission approaches. As presented in Figure 12, with the increase of T_{inlet}, the $h_{overall}$ of the air-film heat conduction gradually increases; nevertheless, the $h_{overall}$ of the contact heat conduction is in a fluctuation within a narrow range, with no obvious growth or decrease trend. When T_{inlet} rises from 473 K to 873 K, the $h_{overall}$ for the air-film heat conduction increases by 16.1% from 71.9 $W{\cdot}m^{-2}{\cdot}K^{-1}$ to 83.5 $W{\cdot}m^{-2}{\cdot}K^{-1}$. Consequently, it can be concluded that the rise of T_{inlet} has a significant promoting effect on the $h_{overall}$ for the air-film heat conduction, yet it has no effect on the $h_{overall}$ for the contact heat conduction. It could be explained that the heat conductivity of the air k_g is an increasing function of temperature in this study, which leads to the enhancement of the heat transmission capacity of the air-film heat conduction when T_{inlet} increases. Whereas the heat conductivity of particle k_s is constant and does not change with temperature, thus the heat transmission capacity for the contact heat conduction does not increase with the rise of T_{inlet}.

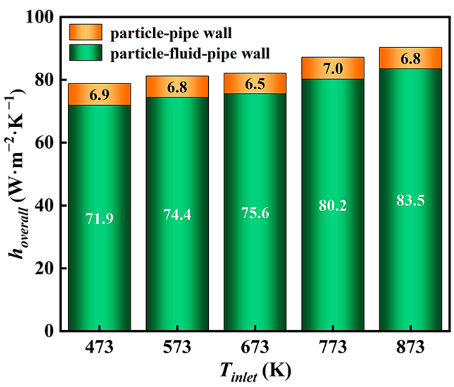

Figure 12. Variation in the overall heat transmission coefficient for the contact heat conduction and the air-film heat conduction with the inlet particle temperature.

In addition, the effect of the inlet particle temperature T_{inlet} on local heat transmission coefficient h_{local}, the local heat transmission coefficient for the air-film heat conduction $h_{local\text{-}pfw}$, and the local heat transmission coefficient for the contact heat conduction $h_{local\text{-}pw}$ are also investigated. Figure 13a is the variation in the local heat transmission coefficient h_{local} with the inlet particle temperature T_{inlet}. It can be observed that with the increase of T_{inlet}, the h_{local} of each local region increases. When the T_{inlet} increases from 473 K to 873 K and from 0° to 150°, the h_{local} of the five local regions increases by 11.6%, 15.2%, 20.5%, 16.3%, and 9.9% respectively. It can be explained that the increase of T_{inlet} results in the rise of particle temperature in each region, which improves the heat conductivity of the air film and enhances the heat transmission capacity. The increase of h_{local} in the 60~90° region is the largest, and the increase of h_{local} in the 30~60° and 90~120° regions are slightly smaller than that in the 60~90° region, while the increase of h_{local} in the 0~30° and 120~150° regions are the smallest.

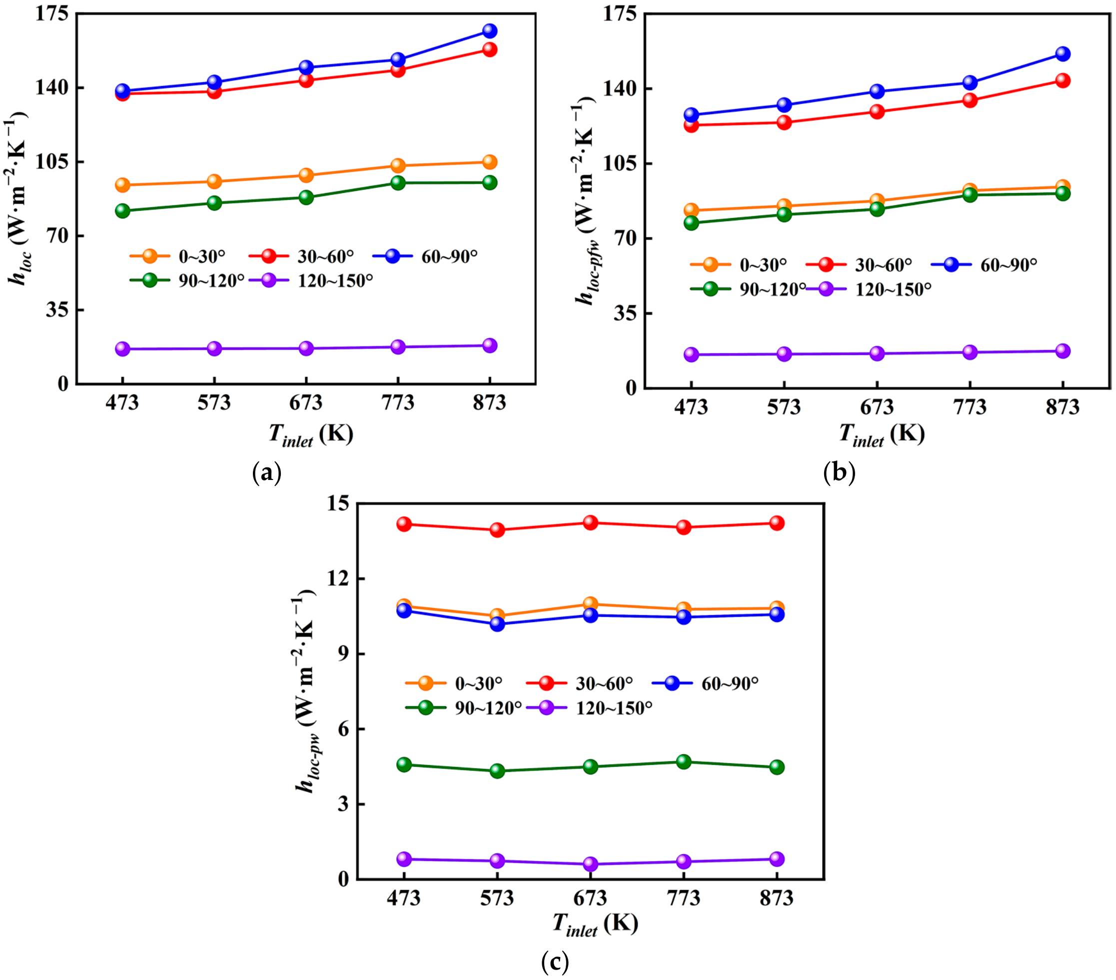

Figure 13. Variation in the local heat transmission coefficient with the inlet particle temperature: (**a**) for both of the air-film heat conduction and the contact heat conduction; (**b**) for the air-film heat conduction; (**c**) for the contact heat conduction.

The differences in the increase in the h_{local} for each local region results from the discrepancy in particle flow characteristics around the heat exchanger pipe. The rise of the h_{local} in the 60~90° region is the largest, because apart from some uncooled high-temperature particles from the top region flowing into it, the high-temperature particles on the side also heat the cooled particles from the upstream. Thus, the higher the T_{inlet}, the higher the particles temperature is in this region and the greater the heat conductivity of the air film. As for the 0~30° region, particles flow tardily here, thus form a stagnation zone where particles stay and be cooled for a long time, resulting in low particle temperature with small air film heat conductivity and inferior heat transmission capacity. As a consequence, the influence of T_{inlet} on this region is smaller than on other regions.

Figure 13b is the variation in the local heat transmission coefficient for air-film heat conduction $h_{loc\text{-}pfw}$ with T_{inlet}. Because of the leading role of this heat transmission approach, the variation tendency of the $h_{loc\text{-}pfw}$ is essentially the same as that of the h_{local} in Figure 13a. Figure 13c presents the variation in the local heat transmission coefficient for contact heat conduction $h_{loc\text{-}pw}$ with T_{inlet}. For the same reason why the $h_{overall}$ for the contact heat conduction is almost unaffected by T_{inlet} as mentioned before, $h_{loc\text{-}pw}$ in each local region only fluctuates in a small range. Compared with Figure 9a–c in Section 3.2.1, the relative sizes of h_{local}, $h_{loc\text{-}pfw}$, and $h_{loc\text{-}pw}$ in each local region of Figure 13a–c do not change, indicating that T_{inlet} does not affect the ranking of the heat transmission coefficient of local regions.

Figure 14 presents the change in the average particle's temperature $T_{p,ave}$ of the five local regions and the overall region of the heat exchanger pipe with the inlet particle temperature T_{inlet}. With the increase of T_{inlet}, the $T_{p,ave}$ of the five local regions and the overall region of the heat exchanger pipe increases. Compared with the growth trend of $T_{p,ave}$ with v_{out} gradually slowing down, the growth trend of $T_{p,ave}$ with T_{inlet} approaches linear. The reason is that v_{out} has an effect on various parameters including particles residence time, collision contact area, and air film heat conductivity caused by particle update frequency; therefore, the growth trend of $T_{p,ave}$ gradually slows down. In the heat transmission algorithm applied in this study, the change of T_{inlet} only affects the heat conductivity of the air film, so the growth trend of $T_{p,ave}$ is close to linear. When the T_{inlet} rises from 473 K to 873 K, the $T_{p,ave}$ of the overall region of the heat exchanger pipe increases from 410.6 K to 664.3 K, with a growth rate of 61.8%.

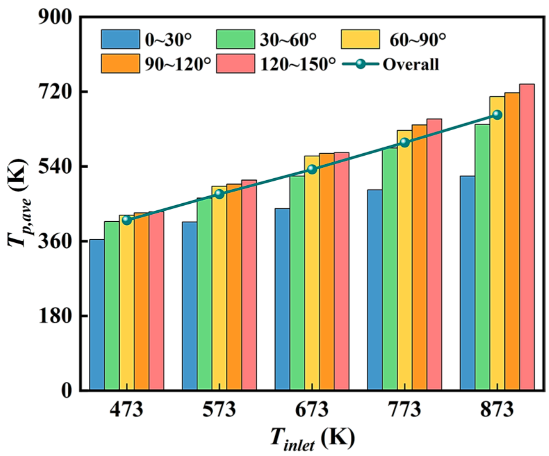

Figure 14. Variation in the local and overall particles average temperature of heat exchanger pipe with the inlet particle temperature.

4. Conclusions

DEM is applied to numerically investigate the flow and heat transmission characteristics of multi-size particles with normal distribution characteristics in a single pipe moving bed heat exchanger. The influence of outlet particle velocity and inlet particle temperature on contact number, particle velocity distribution, heat transmission coefficient and particle temperature distribution are analyzed. The key findings are summarized below:

1. As the outlet particle velocity (v_{out}) rises, the local and the overall particles average tangential velocity (v_{tan}) of heat exchanger pipe increases steadily. When v_{out} increases to 5 mm/s from 1 mm/s, the overall v_{tan} of the heat exchanger pipe increases from 2.7 mm/s to 19.9 mm/s, while the contact number (N_c) of the five local regions and the overall of heat exchanger pipe fluctuates slightly and remains basically steady.

2. v_{out} significantly affects the heat transmission coefficient of the heat exchanger pipe for contact heat conduction and air-film heat conduction. When v_{out} grows to 5 mm/s from 1 mm/s, the $h_{overall}$ of the air-film heat conduction increases by 37.4%, while the $h_{overall}$ of the contact heat conduction increases by 24.2%. In addition, the air-film heat conduction contributes the most to heat transmission and plays a leading role.
3. The inlet particle temperature (T_{inlet}) only affects the heat transmission coefficient for the air-film heat conduction but does not affect that for the contact heat conduction. When T_{inlet} rises from 473 K to 873 K, the $h_{overall}$ of the air-film heat conduction increases by 16.1% from 71.9 W·m^{-2}·K^{-1} to 83.5 W·m^{-2}·K^{-1}. In addition, h_{loc} and $h_{loc\text{-}pfw}$ in 60~90° region are the largest, $h_{loc\text{-}pw}$ in 30~60° region is the largest, and h_{loc}, $h_{loc\text{-}pfw}$, and $h_{loc\text{-}pw}$ in 120~150° region are the smallest.

Through this study, it is discovered that the flow and heat transmission characteristics are complicated; furthermore, increasing the outlet particle velocity and inlet particle temperature significantly rises the heat transmission coefficient, which provides an approach and basis for strengthening the heat transmission effect of multi-size particles in the MBHE. The following study needs to pay more attention to the particles with other size distribution characteristics in the MBHE, because the high temperature particles produced in different industrial processes may be quite different and complex.

Author Contributions: Conceptualization, W.C. and J.H.; methodology, W.C. and H.L.; software, W.C. and S.Y.; validation, W.C., F.Z. and S.Y.; formal analysis, H.L. and S.Y; investigation, W.C. and H.L.; resources, J.H. and S.Y.; data curation, J.H. and H.L.; writing—original draft preparation, W.C. and H.L.; writing—review and editing, W.C. and J.H.; visualization, J.H.; supervision, J.H. and F.Z.; project administration, J.H.; funding acquisition, J.H. and H.W. All authors have read and agreed to the published version of the manuscript.

Funding: This research was funded by the National Natural Science Foundation of China (Grant No. U2102213, No. 51966007) and the Yunnan Fundamental Research Projects (Grant No. 202302AO370018, Grant No. 202001AS070027).

Data Availability Statement: Dataset available on request from the authors.

Conflicts of Interest: The authors declare no conflicts of interest.

Nomenclature

A_{pipe}	surface area of heat exchanger pipe, m^2
$c_{p,i}$	specific heat capacity of particle i, J·kg^{-1}·K^{-1}
D	diameter of heat exchanger pipe, m
d	diameter of particle, m
d_{max}	maximum diameter of particle, m
F_t	tangential force, N
F_n	normal force, N
g	acceleration of gravity, m·s^{-2}
H	height, m
h	heat transmission coefficient of heat exchanger pipe, W·m^{-2}·K^{-1}
$h_{overall}$	overall heat transmission coefficient of heat exchanger pipe, W·m^{-2}·K^{-1}
h_{local}	local heat transmission coefficient of heat exchanger pipe, W·m^{-2}·K^{-1}
$h_{local\text{-}pw}$	local heat transmission coefficient of heat exchanger pipe wall for contact heat conduction, W·m^{-2}·K^{-1}
$h_{local\text{-}pfw}$	local heat transmission coefficient of heat exchanger pipe wall for air-film heat conduction, W·m^{-2}·K^{-1}
I_i	inertial moment of particle i, kg·m^2
i, j	index of particle
k_g	heat conductivity of air, W·m^{-1}·K^{-1}
$k_{g,ref}$	reference value of air heat conductivity, W·m^{-1}·K^{-1}
k_i	heat conductivity of particle i, W·m^{-1}·K^{-1}
k_j	heat conductivity of particle j, W·m^{-1}·K^{-1}
k_s	heat conductivity of particle, W·m^{-1}·K^{-1}

k_{pipe}	heat conductivity of heat exchanger pipe, W·m^{-1}·K^{-1}
L	length, m
l	normal distance from heat exchanger pipe to particle surface, m
l_{ij}	central distance between particle i and particle j, m
m_i	mass of particle i, kg
N_c	number of particles which contact heat exchanger pipe per unit area in each time step
n	number of particles
n_c	number of particles which contact particle i.
Q	heat transmission rate between particle and heat exchanger pipe, W
$Q_{ij}{}^{pp}$	heat transmission rate between particle i and particle j for contact heat conduction, W
$Q_{ij}{}^{pfp}$	heat transmission rate between particle i and particle j for air-film heat conduction, W
Q^{pw}	heat transmission rate between particle and heat exchanger pipe wall for contact heat conduction, W
Q^{pfw}	heat transmission rate between particle and heat exchanger pipe wall for air-film heat conduction, W
R^c	radius of contact area between particle and heat exchanger pipe, m
R_i	radius of particle i, m
R_j	radius of particle j, m
$R_{ij}{}^c$	radius of circular contact area between particle i and particle j, m
$R_{ij}{}^f$	upper limit distance of air-film heat conduction, m
R_{min}	minimum radius of particle i and particle j, m
R_{max}	maximum radius of particle i and particle j, m
r	radial distance, m
r_{in}	radial distance associated with contact area between heat exchanger pipe and particle, m
r_{out}	distance where the particle air film intersects heat exchanger pipe, m
s	minimum conduction distance, m
T_i	temperature of particle i, K
T_{inlet}	inlet particle temperature, K
T_j	temperature of particle j, K
$T_{p,ave}$	average particle temperature, K
T_r	rolling friction torque, N·m
T_t	tangential torque, N·m
T_{pipe}	temperature of heat exchanger pipe, K
t	time, s
v_i	velocity of particle i, m/s
v_{out}	outlet particle velocity, m/s
v_{tan}	average tangential velocity of particles, m/s
W	width, m
Greek symbols	
ω_i	angular velocity of particle i, rad/s
μ	mean particle size, m
σ	standard deviation, m
δ_g	thickness of air film, m
δ_c	overlap between particle and heat exchanger pipe, m
δ_{max}	maximum air film thickness of particle i and particle j, m
θ	angle, deg
Abbreviations	
DEM	discrete element method
PSD	particle size distribution
MBHE	moving bed heat exchanger
tce	ton of standard coal equivalent

References

1. Lin, B.; Zhang, Z.; Ge, F. Energy Conservation in China's Cement Industry. *Sustainability* **2017**, *9*, 668. [CrossRef]
2. Xu, Q.; Xu, K. Statistical Analysis and Prediction of Fatal Accidents in the Metallurgical Industry in China. *Int. J. Environ. Res. Public Health* **2020**, *17*, 3790. [CrossRef]
3. Li, H.; Guo, S.; Wang, B. Analysis on the coordinated development between China's power industry and national economy based on optimal model GM (1, 1). *Energy Procedia* **2012**, *14*, 181–186. [CrossRef]

4. Jiang, J.; Ye, B.; Xie, D.; Li, J.; Miao, L.; Yang, P. Sector decomposition of China's national economic carbon emissions and its policy implication for national ETS development. *Renew. Sustain. Energy Rev.* **2017**, *75*, 855–867. [CrossRef]
5. Wang, M.; Zhang, L.; Su, X.; Lei, Y.; Shen, Q.; Wei, W.; Wang, M. Assessing the technology impact for industry carbon density reduction in China based on C3IAM-Tice. *Nat. Hazards* **2018**, *99*, 1455–1468. [CrossRef]
6. Cao, X.; Wen, Z.; Zhao, X.; Wang, Y.; Zhang, H. Quantitative assessment of energy conservation and emission reduction effects of nationwide industrial symbiosis in China. *Sci. Total Environ.* **2020**, *717*, 137114. [CrossRef] [PubMed]
7. Teng, X.; Zhuang, W.; Liu, F.-p.; Chang, T.-h.; Chiu, Y.-h. China's path of carbon neutralization to develop green energy and improve energy efficiency. *Renew. Energy* **2023**, *206*, 397–408. [CrossRef]
8. Cheng, Z.; Tan, Z.; Guo, Z.; Yang, J.; Wang, Q. Technologies and fundamentals of waste heat recovery from high-temperature solid granular materials. *Appl. Therm. Eng.* **2020**, *179*, 115703. [CrossRef]
9. Zheng, X.; Lu, X.; Li, J.; Wang, Q.; Kang, Y.; Dong, Z.; Fan, X.; Liu, Z.; Zhang, Y.; Yang, Z.; et al. A novel thin-layer ash reciprocation heat recovery system for bottom ash from circulating fluidized bed boilers: Experimental study. *Appl. Therm. Eng.* **2021**, *183*, 116147. [CrossRef]
10. Zuo, Z.; Feng, Y.; Dong, X.; Luo, S.; Ren, D.; Wang, W.; Wu, Y.; Yu, Q.; Lin, H.; Lin, X. Advances in recovery of valuable metals and waste heat from copper slag. *Fuel Process. Technol.* **2022**, *235*, 107361. [CrossRef]
11. Wang, X.; Feng, Z. Study on affecting factors and standard of rural household energy consumption in China. *Renew. Sustain. Energy Rev.* **2005**, *9*, 101–110. [CrossRef]
12. Almendros-Ibáñez, J.A.; Fernández-Torrijos, M.; Díaz-Heras, M.; Belmonte, J.F.; Sobrino, C. A review of solar thermal energy storage in beds of particles: Packed and fluidized beds. *Sol. Energy* **2019**, *192*, 193–237. [CrossRef]
13. Arena, U.; Di Gregorio, F. Fluidized bed gasification of industrial solid recovered fuels. *Waste Manag.* **2016**, *50*, 86–92. [CrossRef] [PubMed]
14. Liu, Y.; Yang, J.; Wang, J.-y.; Ding, X.-g.; Cheng, Z.-l.; Wang, Q.-w. Prediction, parametric analysis and bi-objective optimization of waste heat utilization in sinter cooling bed using evolutionary algorithm. *Energy* **2015**, *90*, 24–35. [CrossRef]
15. Guo, Z.; Tian, X.; Wu, Z.; Yang, J.; Wang, Q. Heat transfer of granular flow around aligned tube bank in moving bed: Experimental study and theoretical prediction by thermal resistance model. *Energy Conv. Manag.* **2022**, *257*, 115435. [CrossRef]
16. Bartsch, P.; Zunft, S. Granular flow around the horizontal tubes of a particle heat exchanger: DEM-simulation and experimental validation. *Sol. Energy* **2019**, *182*, 48–56. [CrossRef]
17. Liu, J.; Yu, Q.; Peng, J.; Hu, X.; Duan, W. Thermal energy recovery from high-temperature blast furnace slag particles. *Int. Commun. Heat Mass Transf.* **2015**, *69*, 23–28. [CrossRef]
18. Tian, X.; Yang, J.; Guo, Z.; Wang, Q.; Sunden, B. Numerical study of heat transfer in gravity-driven dense particle flow around a hexagonal tube. *Powder Technol.* **2020**, *367*, 285–295. [CrossRef]
19. Guo, Z.; Yang, J.; Tan, Z.; Tian, X.; Wang, Q. Numerical study on gravity-driven granular flow around tube out-wall: Effect of tube inclination on the heat transfer. *Int. J. Heat Mass Transf.* **2021**, *174*, 121296. [CrossRef]
20. Shen, Y.; Sun, P.; Zhang, Z.; Wang, Y.; Zheng, B. A tube heat transfer prediction model considering static friction coefficient of dense particle flow. *Int. J. Heat Mass Transf.* **2023**, *205*, 123902. [CrossRef]
21. Qiu, L.; Sang, D.; Feng, Y.; Huang, H.; Zhang, X. Study on heat transfer of process intensification in moving bed reactor based on the discrete element method. *Chem. Eng. Process.* **2020**, *151*, 107915. [CrossRef]
22. Zhang, H.; Wang, H.; Zhu, X.; Qiu, Y.-J.; Li, K.; Chen, R.; Liao, Q. A review of waste heat recovery technologies towards molten slag in steel industry. *Appl. Energy* **2013**, *112*, 956–966. [CrossRef]
23. Liu, J.; Yu, Q.; Zuo, Z.; Duan, W.; Han, Z.; Qin, Q.; Yang, F. Experimental investigation on molten slag granulation for waste heat recovery from various metallurgical slags. *Appl. Therm. Eng.* **2016**, *103*, 1112–1118. [CrossRef]
24. Zhang, S.; Zhao, L.; Feng, J.; Dong, H. Numerical investigation of the air-particles heat transfer characteristics of moving bed—Effect of particle size distribution. *Int. J. Heat Mass Transf.* **2022**, *182*, 122036. [CrossRef]
25. Qiu, L.; Sang, D.; Li, Y.; Feng, Y.; Zhang, X. Numerical simulation of gas–solid heat transfer characteristics of porous structure composed of high-temperature particles in moving bed. *Appl. Therm. Eng.* **2020**, *181*, 115925. [CrossRef]
26. Zhang, J.; Tian, X.; Guo, Z.; Yang, J.; Wang, Q. Numerical study of heat transfer for gravity-driven binary size particle flow around circular tube. *Powder Technol.* **2023**, *413*, 118070. [CrossRef]
27. Chew, J.W.; Wolz, J.R.; Hrenya, C.M. Axial segregation in bubbling gas-fluidized beds with Gaussian and lognormal distributions of Geldart Group B particles. *AICHE J.* **2010**, *56*, 3049–3061. [CrossRef]
28. Rasteh, M.; Farhadi, F.; Ahmadi, G. Empirical models for minimum fluidization velocity of particles with different size distribution in tapered fluidized beds. *Powder Technol.* **2018**, *338*, 563–575. [CrossRef]
29. Jiang, F.; Liu, Y.; Wang, H.; Qi, G.; Nkomazana, P.; Li, X. Effect of particle characteristics on particle collision behaviors and heat transfer performance in a down-flow circulating fluidized bed evaporator. *Powder Technol.* **2022**, *399*, 116954. [CrossRef]
30. Cundall, P.A.; Strack, O.D. A discrete numerical model for granular assemblies. *Geotechnique* **1979**, *29*, 47–65. [CrossRef]
31. Hoomans, B.P.B. *Granular Dynamics of Gas-Solid Two-Phase Flows*; Universiteit Twente Enschede: Enschede, The Netherlands, 2000.
32. Elghannay, H.A.; Tafti, D.K. Alternate tangential impact treatments for the soft-sphere collision model. *Part. Sci. Technol.* **2019**, *38*, 354–364. [CrossRef]
33. Feng, Y.-H.; Zhang, Z.; Qiu, L.; Zhang, X.-X. Heat recovery process modelling of semi-molten blast furnace slag in a moving bed using XDEM. *Energy* **2019**, *186*, 115876. [CrossRef]

34. Guo, Z.; Zhang, S.; Tian, X.; Yang, J.; Wang, Q. Numerical investigation of tube oscillation in gravity-driven granular flow with heat transfer by discrete element method. *Energy* **2020**, *207*, 118203. [CrossRef]
35. Deng, S.; Wen, Z.; Lou, G.; Zhang, D.; Su, F.; Liu, X.; Dou, R. Process of particles flow across staggered tubes in moving bed. *Chem. Eng. Sci.* **2020**, *217*, 115507. [CrossRef]
36. Musser, J.M. Modeling of Heat Transfer and Reactive Chemistry for Particles in Gas-Solid Flow Utilizing Continuum-Discrete Methodology (CDM). Ph.D. Thesis, West Virginia University, Morgantown, WV, USA, 2011.
37. Hertel, J.D.; Zunft, S. Experimental validation of a continuum model for local heat transfer in shell-and-tube moving-bed heat exchangers. *Appl. Therm. Eng.* **2022**, *206*, 118092. [CrossRef]
38. Albrecht, K.J.; Ho, C.K. Design and operating considerations for a shell-and-plate, moving packed-bed, particle-to-sCO2 heat exchanger. *Sol. Energy* **2019**, *178*, 331–340. [CrossRef]
39. Zheng, B.; Sun, P.; Liu, Y.; Zhao, Q. Heat transfer of calcined petroleum coke and heat exchange tube for calcined petroleum coke waste heat recovery. *Energy* **2018**, *155*, 56–65. [CrossRef]
40. Batchelor, G.K.; O'brien, R. Thermal or electrical conduction through a granular material. *Proc. R. Soc. Lond. Ser. A* **1977**, *355*, 313–333. [CrossRef]
41. Rong, D.; Horio, M. DEM simulation of char combustion in a fluidized bed. In Proceedings of the Second International Conference on CFD in the Minerals and Process Industries CSIRO, Melbourne, Australia, 6–8 December 1999.
42. Xavier, A.; Davidson, J. *Fluidization*; Cambridge University Press: Cambridge, UK, 1978; pp. 333–338.
43. Morris, A.; Pannala, S.; Ma, Z.; Hrenya, C. A conductive heat transfer model for particle flows over immersed surfaces. *Int. J. Heat Mass Transf.* **2015**, *89*, 1277–1289. [CrossRef]
44. Morris, A.; Ma, Z.; Pannala, S.; Hrenya, C. Simulations of heat transfer to solid particles flowing through an array of heated tubes. *Sol. Energy* **2016**, *130*, 101–115. [CrossRef]
45. Zhang, R.; Yang, H.; Lu, j.; Wu, Y. Theoretical and experimental analysis of bed-to-wall heat transfer in heat recovery processing. *Powder Technol.* **2013**, *249*, 186–195. [CrossRef]
46. Okazaki, M.; Yamasaki, T.; Gotoh, S.; Toei, R. Effective Thermal Conductivity for Granular Beds of Various Binary Mixtures. *J. Chem. Eng. Jpn.* **1981**, *14*, 183–189. [CrossRef]
47. Dai, Y.L.; Liu, X.J.; Xia, D. Flow characteristics of three typical granular materials in near 2D moving beds. *Powder Technol.* **2020**, *373*, 220–231. [CrossRef]
48. Guo, Z.; Tian, X.; Yang, J.; Shi, T.; Wang, Q. Comparison of Heat Transfer in Gravity-Driven Granular Flow near Different Surfaces. *J. Therm. Sci.* **2020**, *30*, 441–450. [CrossRef]
49. Tian, X.; Zhu, F.; Guo, Z.; Zhang, J.; Yang, J.; Wang, Q. Numerical investigation of gravity-driven particle flow along the trapezoidal corrugated plate for a moving packed bed heat exchanger. *Powder Technol.* **2022**, *405*, 117526. [CrossRef]
50. Xiao, P.-H.; Li, B.-W.; Sun, Y.-S. A model to determine the overall bed-to-wall heat transfer coefficient and its influence factor analysis in moving bed. *Int. J. Heat Mass Transf.* **2020**, *154*, 119655. [CrossRef]